Heritage Science

RESEARCH Open Access

Urban sprawl analysis of Akhmim city (Egypt) and its risk to buried heritage sites: insights from geochemistry and geospatial analysis

Mohammed Hagage[1*], Ahmed A. Madani[2], Ahmed Aboelyamin[3] and Salwa F. Elbeih[1]

Abstract

The present study employs a multidisciplinary approach to highlight the risks of urban expansion on buried cultural heritage sites. The buried temple of Ramses II in Akhmim city was chosen as a case study to assess the impact of urban expansion on its preservation. Support Vector Machine (SVM) classification was utilized to analyze satellite images from multiple sensors and evaluate the extent of urban growth surrounding the temple. The study also incorporated petrographic and mineralogical analyses of statues discovered in the temple, along with calculations of saturation indices, to assess the potential interactions between groundwater and archaeological materials. The findings indicate that urban development is encroaching upon the temple, posing potential risks to its preservation. Saturation indices for minerals in groundwater indicate a high tendency to dissolve dolomite (a common mineral in limestone) and to precipitate halite (sodium chloride). This is a concern because the artifacts unearthed from the temple are primarily composed of limestone. Consequently, there is a risk to the artifacts due to erosion and disintegration caused by mineral crystallization and expansion, as evidenced by the analysis of the rock and mineral characteristics of the statues discovered in the temple. The study proposes protective measures for the temple, including defining its dimensions beneath the urban area and establishing a dedicated protection zone around it.

Keywords Urban expansion, Cultural heritage preservation, CORONA satellite, Land use evolution, Support Vector Machine (SVM) classification, Groundwater saturation indices

Introduction

Protection of heritage sites has become a top priority for many countries due to their cultural and economic importance [1]. The World Heritage Convention, which was adopted in 1972, is the most important global instrument for establishing this notion and bringing nations together in pursuit of cultural heritage protection [2]. Preserving and protecting these sites is essential because they are considered to be of outstanding cultural significance to the common heritage of humanity [3]. Cultural heritage sites are at risk of destruction due to various natural and human-induced factors. These include climate change [4], natural disasters [5], pollution [6], urbanization [7], and terrorism [8].

More than half of the world's population currently lives in urban areas, and this trend is expected to continue [9]. By 2050, it is projected that over two-thirds of the world's population will live in cities [10]. This urban expansion has led to various environmental, social, and economic

*Correspondence:
Mohammed Hagage
mohammedhagage123@gmail.com; mohammed.hagage@narss.sci.eg
[1] National Authority for Remote Sensing and Space Sciences (NARSS), Cairo 11765, Egypt
[2] Geology Department, Faculty of Science, Cairo University, Giza 12613, Egypt
[3] Conservation Department, Ministry of antiquities, Sohag 82511, Egypt

changes that affect both developed and developing nations [11]. As urbanization continues, it increasingly affects cultural heritage sites, including buried archaeological sites [12, 13]. Therefore, it is crucial to pay particular attention to the impact of urbanization on cultural heritage sites and find ways to protect them for future generations [14].

Egypt's population in urban areas has been rapidly increasing, from 10 million in 1960 to 42 million in 2018, and is expected to double by 2030 [15]. This growth necessitates more urban expansion, which is often uncontrolled and has direct or indirect impacts on Egypt's cultural heritage sites [16, 17]. Therefore, it is crucial to investigate the cultural heritage-related dimensions of urban development and address the impact of urban expansion on cultural heritage sites [18]. The rapid urban growth in Egypt, particularly during the unstable period in January 2011, posed a significant threat to the archaeological areas located within residential areas [19]. To counter these threats, continuous monitoring of urban growth in terms of the type and extent of changes occurring over time is essential for supporting planners and decision-makers [20].

Buried monumental sites are a crucial part of our history and culture, but they are also particularly vulnerable to the negative impacts of urban expansion. As cities grow, these sites are often threatened by development and construction, and subsoil water can be an aggressive deterioration factor [21]. Groundwater can cause the deterioration of archaeological sites, which includes the loss of the surface layers of stone that carry engravings, soil salinization, crystallization of salts in walls and columns, stone bleeding, destruction of wall paintings and texts, decreased durability of monumental stones, and seepage of capillary groundwater [22, 23]. Therefore, it is crucial that we prioritize the protection of these sites and work to mitigate the risks of urban expansion [24, 25]. To achieve this, it is necessary to monitor deterioration processes over relatively short time intervals, and determining the parameters that control them is essential for mitigating potential risks [26].

The use of machine learning has become essential in various environmental studies due to its ability to integrate and analyze large datasets, which significantly and effectively contributes to leveraging and presenting the data clearly [27–29]. Support Vector Machine (SVM) is one of the most widely used machine learning algorithms for studying land use using satellite imagery [30]. Satellite images from different time periods provide an invaluable resource for monitoring urban growth [31]. In recent times, satellite data and GIS have made significant contributions to various aspects of archaeological studies, including archaeological site discovery [32], archaeological site management [33], monitoring natural and anthropogenic risks on archaeological sites [34], geo-environmental risk assessment [35, 36], and archaeological site mapping [37, 38].

Geochemical techniques play a crucial role in the study of archaeological building materials and identification of their deterioration, particularly when influenced by groundwater [39]. Through the application of various geochemical analyses and investigations, valuable insights can be gained regarding the composition, alteration processes, and degradation mechanisms of these materials [40]. Techniques such as X-Ray Diffraction (XRD) and scanning electron microscopy (SEM) enable the identification and characterization of mineral phases present in archaeological building materials [41]. By examining the mineralogical composition, it is possible to determine the susceptibility of materials to degradation processes induced by groundwater, such as dissolution, mineral leaching, and salt crystallization [42]. The use of software, such as PHREEQC, aids in simulating the interactions between groundwater and building materials [43]. By incorporating data on the chemical composition of groundwater and the mineralogical composition of materials, potential degradation pathways can be predicted, and the long-term impact of groundwater on materials can be assessed [22].

Akhmim is an ancient city with a history dating back approximately to 6000 years. The ancient archaeological city lies beneath the modern city of Akhmim, and only one archaeological site that testifies to its past has been discovered. This site is part of a temple dating back to Ramses II (1303–1213 BC). A section of this temple was discovered in 1981, while the rest of the temple is still buried under modern buildings. Therefore, this paper aims to analyze the urban sprawl of Akhmim city and its influence on the buried temple of Ramses II through the following objectives:

1. Using satellite data and Support Vector Machine (SVM) algorithm to analyze urban expansion over the past 55 years.
2. Utilizing geochemical techniques to determine the deterioration of archaeological building materials as a result of burial.
3. Presenting a proposal to protect the temple from further urban expansion.

The findings of this research will contribute to the ongoing debate on the importance of preserving cultural heritage sites in the face of rapid urban expansion and raise awareness among policymakers, urban planners, and the public regarding the importance of urban

development and the need to protect Egypt's invaluable historical assets for future generations.

Materials and methods

Buried temple of Ramses II in Akhmim

Akhmim is an ancient city located on the eastern bank of the River Nile, Sohag Governorate, approximately 450 km south of Cairo (Fig. 1). It has a history dating back approximately to 6000 years [44], and it was known as Ipu or Khent-min to the ancient Egyptians and as Panopolis to the Greeks [45]. Akhmim was a cultural center dedicated to the principal god Min, and it served as the capital of the Ninth Upper Egyptian Nome during the dynastic period of ancient Egypt [46].

The ancient archaeological city lies beneath the modern Akhmim city, and only one archaeological site that testifies to its past has been discovered. This site is part of a temple dating back to Ramses II (1303-1213 BC) [47]. The temple, described by Herodotus (c. 450 BC) as having a stone enclosure, two colossal statues, and palm trees, was in good condition in medieval times, and some of it remains survived until the nineteenth century [48]. It was described as one of the wonders of the world in many accounts [49].

In 1981, a section of the temple that included a statue of Ramses II and a giant statue of his daughter Merit-Amun was uncovered. Subsequent excavations in 1991 revealed parts of a seated colossus of Ramses II, which was surrounded by mud brick walls [50]. The discovered section of the temple was converted into an open-air museum in 1995 (Fig. 2), while the remaining parts of the temple are still buried under buildings [51].

The motivation behind this study stems from the urgent need to address the potential threats posed by urban sprawl on the buried heritage sites in Akhmim city. As urban expansion continues, there is a significant risk of irreversible damage to the buried temple of Ramses II, which represents an invaluable historical and cultural treasure. Figure 3 shows a simplified flowchart of the methodology used and the most important results and recommendations.

Geospatial analysis

To investigate the urban expansion in Akhmim city over the past 55 years, this study relied on multispectral

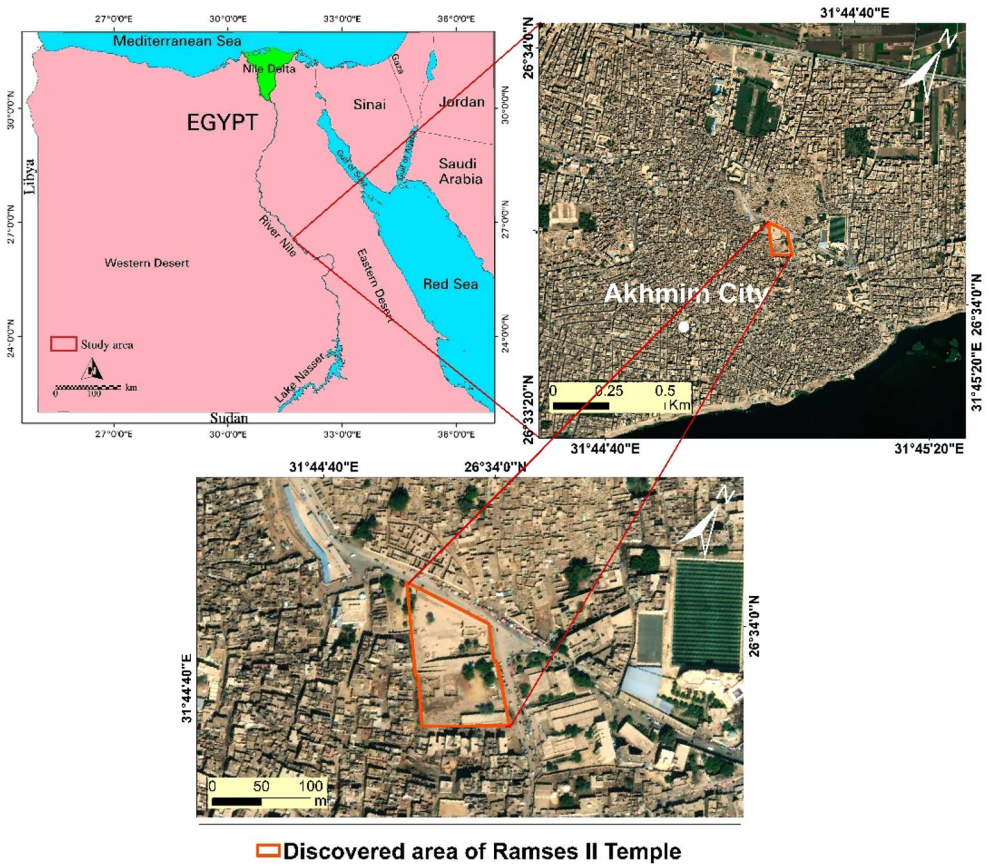

Fig.1 Akhmim city and the discovered area of Ramses II temple by WorldView-3 satellite image

Fig.2 The discovered section of the Ramses II temple (the Open-Air Museum)

satellite images from two different satellites (Landsat 5 and Sentinel 2A) and the panchromatic CORONA images. In addition, topographic analysis was performed using the ALOS PALSAR digital elevation model (Table 1). Using a high-resolution WorldView-3 satellite image, the temple of Ramses II at Akhmim was reconstructed based on the locations of the discovered parts of the temple, as well as the design of the temples during the reign of Ramses II, within the ArcGIS software environment. The processing of satellite images was carried out using ENVI software and the Sentinel Application Platform (SNAP). All cartographic work and topographic analysis were completed with the aid of ArcGIS Desktop 10.5 software.

The land cover in the study area was classified into four classes, namely urban areas, agricultural areas, Nile River, and bare land, based on the visual interpretation and spectral diversity of the satellite images used. The classification process involved four stages: defining training data (training samples) to represent the spectral signature of the classified classes, evaluation of training data, classification using Support Vector Machine (SVM), and classification accuracy assessment. The selection of training samples was based on the image interpretation and spectral analysis of each class.

SVM is a supervised classification machine learning method derived from statistical learning theory [52]. SVM has been widely used to classify optical and radar satellite data and has demonstrated high effectiveness in terms of classification speed and accuracy [53]. SVM is designed to define the optimal separation margin that divides the dataset into several classes based on the input training samples [54]. When using a SVM classifier in thematic mapping, the user needs to specify which kernel to use to improve the separability and reduce classification errors [55], where the classification accuracy is highly dependent on the choice of kernel function [56]. Users can choose between polynomial, the radial basis function (RBF), and the sigmoid [57]. In remote sensing studies, the polynomial and RBF kernel are the most common and are known to work well [53, 58]. However, for LULC classification, RBF is the most popular technique and gives better accuracy compared with the other methods [54, 59, 60]. In this study, the SVM classification technique was performed in ENVI software version 5.3 with the RBF kernel. The SVM parameter values used were 0.01 for the Gamma in the kernel function and 100 for the penalty parameter. The pyramid parameter was set to zero, and the classification probability threshold was also set to zero to ensure that each image pixel receives only one class label, and no pixel remains unclassified.

For the classification accuracy assessment, the confusion matrix using the ground truth Region Of Interest (ROIs) tool in ENVI software was utilized. This matrix was based on ground truth points that represented the different land cover classes in the study area. The ground truth points were obtained through a field visit (for the 2022 classification) and visual interpretation of the images used (for the 1985 classification). The classification accuracy results were presented using the overall accuracy (OA) and kappa (ki) coefficient. The overall accuracy was calculated by summing the number of correctly classified values and dividing it by the total number of values. The kappa coefficient measures the agreement between the classification and truth values (as shown in Eq. 1). The kappa coefficient measures the agreement between the classification and truth values (Eq. 1). A kappa value of 1 represents perfect agreement, while a value of 0 represents no agreement.

$$K = \frac{N\sum_{i=1}^{n} m_{i,i} - \sum_{i=1}^{n}(G_i C_i)}{N^2 - \sum_{i=1}^{n}(G_i G C_i)} \quad (1)$$

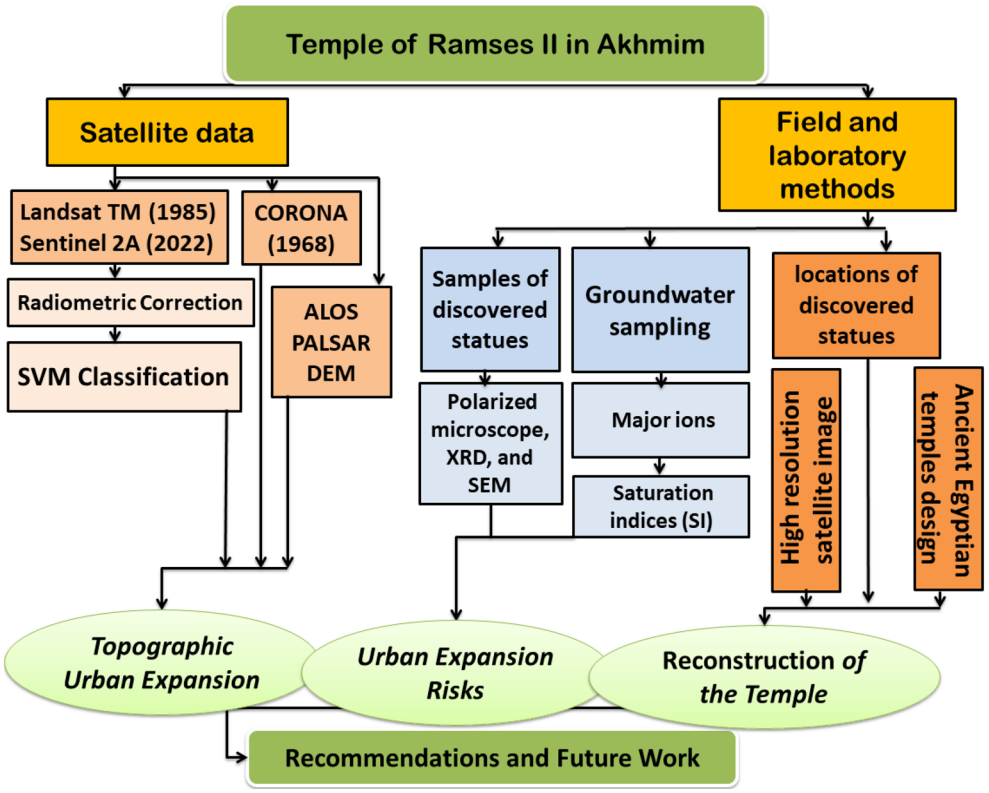

Fig.3 Flowchart of the methodology used and the most important results and recommendations

Table 1 Properties of remote sensing data used

1. Satellite images					
No	**Satellite ID**	**Sensor ID**	**Spatial resolution**	**Acquisition date**	**Source**
1	CORONA	KH-4B	2.1 m	Nov 1968	https://corona.cast.uark.edu
2	Landsat 5	TM	30 m	Aug 1985	https://earthexplorer.usgs.gov/
3	WorldView-3	WV110	1.24 m	Oct 2017	https://worldview3.digitalglobe.com/
4	Sentinel	2A	10 m	Oct 2022	https://scihub.copernicus.eu/
2. Digital elevation model (DEM)					
No	**Product**	**Spatial resolution**	**Acquisition date**	**Source**	
1	ALOS PALSAR	12.5 m	Feb 10, 2007	https://search.asf.alaska.edu/#/	

where; i represents the class number, N denotes the total number of classified values compared to truth values, $m_{i,i}$ signifies the number of values belonging to the truth class i that have also been classified as class i (i.e., values found along the diagonal of the confusion matrix),C_i stands for the total number of predicted values belonging to class i, and G_i represents the total number of truth values belonging to class i.

Groundwater saturation indices

Except for the discovered section, the temple of Ramses II in Akhmim is currently buried under the buildings, leaving building materials vulnerable to deterioration from salts present in the soil and groundwater. A groundwater sample was collected from the vicinity of the Open-Air Museum in Akhmim to study its chemical properties and the impacts it may have on building materials. The samples were chemically analyzed to determine the concentration of major ions.

The saturation indexes (SI) of different minerals in the groundwater sample were also calculated to identify the possible interactions between the groundwater and archaeological building materials, using the equation developed by [61]:

$$SI = \log\left(\frac{K_{IAP}}{K_{SP}}\right) \quad (2)$$

where K_{sp} is the solubility product and K_{IAP} is the ion activity product.

Saturation indices are a measure of whether water is in equilibrium with a solid phase or if it is unsaturated or supersaturated in relation to solids [62]. The saturation index can be used to determine whether water is corrosive to materials or causes scaling on surfaces [63]. It can also be used to determine whether water will cause a particular mineral to form solid deposits [64]. When SI is equal to zero, the water is in equilibrium with the mineral phase. SI values below zero (negative values) indicate under saturation, and that the mineral phase tends to dissolve, while SI values above zero (positive values) indicate oversaturation, and the mineral phase tends to precipitate [65].

Archaeological building materials analysis

To study the petrographic and mineralogical properties of the building materials, five samples were taken from the statues detected in the temple. Two samples were taken from the Merit Amun statue (a sample of the statue and a salt sample from the pedestal), two samples were taken from the Ramses II statue (a sample of the statue and a salt sample from the statue), and a sample was taken from the colossal seated statue of Ramses II. Petrographic and mineralogical properties of the samples were studied using a polarized microscope, X-Ray Diffraction (XRD), and Scanning Electron Microscope (SEM).

Results and discussion

Topographic urban expansion

To assess the spatial extent of urban expansion and its potential impact on buried heritage sites, the land cover was classified using the SVM model. Table 2 presents the ground truth values and the corresponding predicted values for the agricultural areas, water bodies, urban areas, and bare land classes in 1985 and 2022. The overall accuracy, calculated by summing the number of correctly classified values and dividing it by the total number of values, was 93.5% for the 1985 images and 97.4% for the 2022 images. The kappa coefficient, which measures the agreement between the classification and ground truth values, was 0.92 for 1985 and 0.96 for 2022. These values indicate a high level of agreement between the SVM classification and the true land cover classes.

The producer accuracy represents the percentage of correctly classified values for each class. In the 1985 images, the producer accuracy was 100% for agricultural areas and water bodies, 88.7% for urban areas, and 85.2% for bare land. In the 2022 images, the producer accuracy got improved to be 100% for agricultural areas and water bodies, 92.4% for urban areas, and 97.3% for bare land. These high accuracy values indicate the effectiveness of the SVM model in classifying the land cover in the study area.

These results highlight the effectiveness of the SVM model in accurately classifying the land cover in the study area. The high classification accuracy and strong agreement with the ground truth values demonstrate the reliability of the SVM analysis in identifying and mapping the different land cover classes, including urban areas, agricultural areas, water bodies, and bare land.

Table 2 Summary of accuracy (%) and Kappa coefficient of the 1985 and 2022 SVM classification

Class Name	Ground Truth (1985)				Ground Truth (2022)			
	Agricultural areas	Water bodies	Urban areas	Bare land	Agricultural areas	Water bodies	Urban areas	Bare land
Agricultural areas	100	0	0	0	100	0	0	0
Water bodies	0	100	0	0	0	100	0	0
Urban areas	0	0	88.7	14.8	0	0	92.4	2.7
Bare land	0	0	11.3	85.2	0	0	7.6	97.3
Total	100	100	100	100	100	100	100	100
Producer Accuracy	100%	100%	88.7%	85.2%	100%	100%	92.4%	97.3%
Overall Accuracy	93.5%				97.4%			
Kappa Coefficient	0.92				0.96			

These findings contribute to our understanding of urban sprawl in Akhmim city and the associated risks to buried heritage sites. By providing precise land cover classification, the SVM analysis aids in identifying areas of urban encroachment. This allows for informed decision-making and the implementation of protective measures to mitigate the risks posed to the cultural heritage in Akhmim city.

The digital elevation model of Akhmim city clearly shows an elevated area in the center of the modern city, which could possibly be the location of the ancient city (Fig. 4A). The ancient city was constructed on elevated areas as they provided a natural defense against Nile floods and enemies. Furthermore, these elevated areas offered better drainage and ventilation systems, making them more habitable for human settlements. The CORONA satellite image revealed that the urban area in 1968 covered an area of approximately 0.94 km^2, mainly concentrated in the elevated area to the south of the archaeological discovery site (Fig. 4B). At that time, the archaeological site was a barren land situated at the northeastern edge of Akhmim city.

The construction of the Aswan High Dam, which was completed in 1970, helped to control the annual flooding of the River Nile. As a result, large tracts of land that were previously flooded are now available for

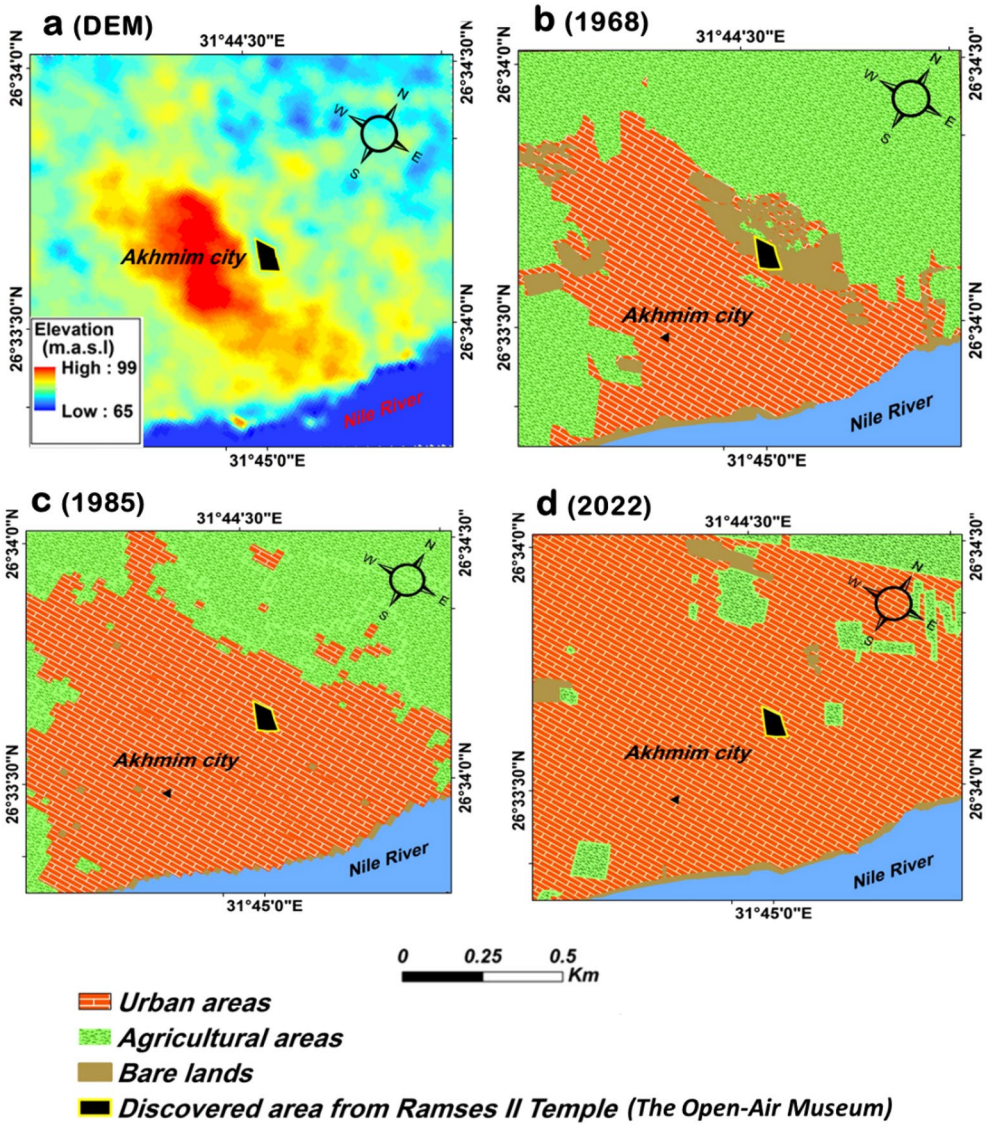

Fig. 4 **a** Land surface elevation for Akhmim city using the ALOS PALSAR High-Resolution DEM (12.5 m), **b**, **c**, **d** Land use in Akhmim city in 1968, 1985, and 2022

agriculture and urban development. The expansion of cities in Egypt after the construction of the High Dam was driven by several factors, including population growth, increased economic opportunities, and the availability of new lands for development.

Among the ancient cities in Egypt that witnessed a great urban expansion after the construction of the High Dam is the city of Akhmim. The Landsat satellite image in 1985 (15 years after the operation of the Aswan High Dam) demonstrated an increase in urban areas to 1.43 km^2, representing an increase of approximately 0.5 km^2 compared with 1968 (Fig. 4C). Urban expansion extended to the north in the direction of the discovered area of the temple, where the urban areas surrounded the archaeological area from all sides.

Urban expansion around the archaeological area has continued until now, as a Sentinel 2 satellite image revealed an increase in urban areas in 2022 to approximately 2.1 km^2 (Fig. 4D), an increase of approximately 0.7 km^2 from 1985 and an increase of 1.15 km^2 from 1968 (Table 3). With the continued urban growth, the discovered section of the temple became surrounded by a high urban density, because of which the exploration of other parts of the temple stopped. This expansion poses great challenges to the preservation of the temple and the management of the discovered section of it.

Urban expansion risks

The rapid urban expansion has had negative impacts on the environment and cultural heritage of the region. Apart from the discovered section, the presence of Akhmim temple below the urban area with high urban density exposes it to great risks, the most important of which are the deterioration of building materials due to groundwater and burial soil, and the hindrance of excavations, along with the increased illegal exploration by robbers.

Petrographic examination of a sample taken from the Merit Amun statue under a polarizing microscope indicated that it is micritic limestone. XRD results indicated that it is composed of 93% calcite mineral ($CaCO_3$) and 3% dolomite mineral ($CaMg(CO_3)_2$). XRD results for a salt sample taken from the pedestal indicated that it consists of 93% halite mineral (NaCl) with a small percentage of calcite mineral (4%) and quartz mineral (Fig. 5A, B).

Petrographic examination of a sample taken from the Ramses II statue under a polarizing microscope indicated that it is micritic limestone. XRD results indicated that it is composed of 92% calcite mineral ($CaCO_3$) with a small percentage of dolomite mineral (5%) and smectite mineral (3%). XRD results for a salt sample taken from the statue indicated that it consists of 96% halite mineral (NaCl) and 4% calcite mineral (Fig. 5C, D).

Petrographic examination of a sample taken from the colossal seated statue of Ramses II under a polarizing microscope indicated that it is biomicritic limestone. XRD results indicated that it is composed of 88% calcite mineral ($CaCO_3$) with small percentages of halite mineral (6%), illite mineral (3%), and smectite mineral (3%). Examination of the sample using SEM showed the diffusion of sodium chloride salts (NaCl) between calcite crystals (Fig. 5E, F). The source of this salt is likely to be burial soil, groundwater, and sewage seepage from homes built within the archaeological area.

The chemical analysis of groundwater in the vicinity of the Open-Air Museum in Akhmim City revealed the presence of numerous ions and minerals that have the potential to impact archaeological building materials. The total dissolved solids (TDS) concentration in the groundwater near the Open-Air Museum is about 950 mg/L, which is significantly higher than the TDS concentration in groundwater wells located in wilderness area, which is about 400 mg/L, as illustrated in Table 4. This disparity in total dissolved solids levels can be attributed to human activities such as industrial discharges and domestic wastewater [66–68]. High concentrations of dissolved salts in groundwater can significantly impact building materials. When water containing dissolved salts evaporates, the salts are left behind and can accumulate on the surface, causing discoloration, warping, and even structural damage. Additionally, dissolved salts can react with building materials, resulting in chemical changes that can weaken the structure [69]. Chloride ions can cause corrosion and pitting on the surface of stones [70]. Nitrates can also form on stone surfaces due to the presence of nitrate, ammonia, and ammonium salts, which can lead to discoloration and loss of detail on the stone surface [71].

Table 4 presents the results of saturation indices for minerals in groundwater. The positive saturation indices for calcite and aragonite suggest that the groundwater is supersaturated with respect to these minerals. This

Table 3 Urban expansion in the Akhmim city from 1968 to 2022

Land use (km^2)	1968	1985	2022	Urban expansion between		
				1968 and 1985	1985 and 2022	1968 and 2022
Urban areas	0.94	1.43	2.1	0.49	0.67	1.15

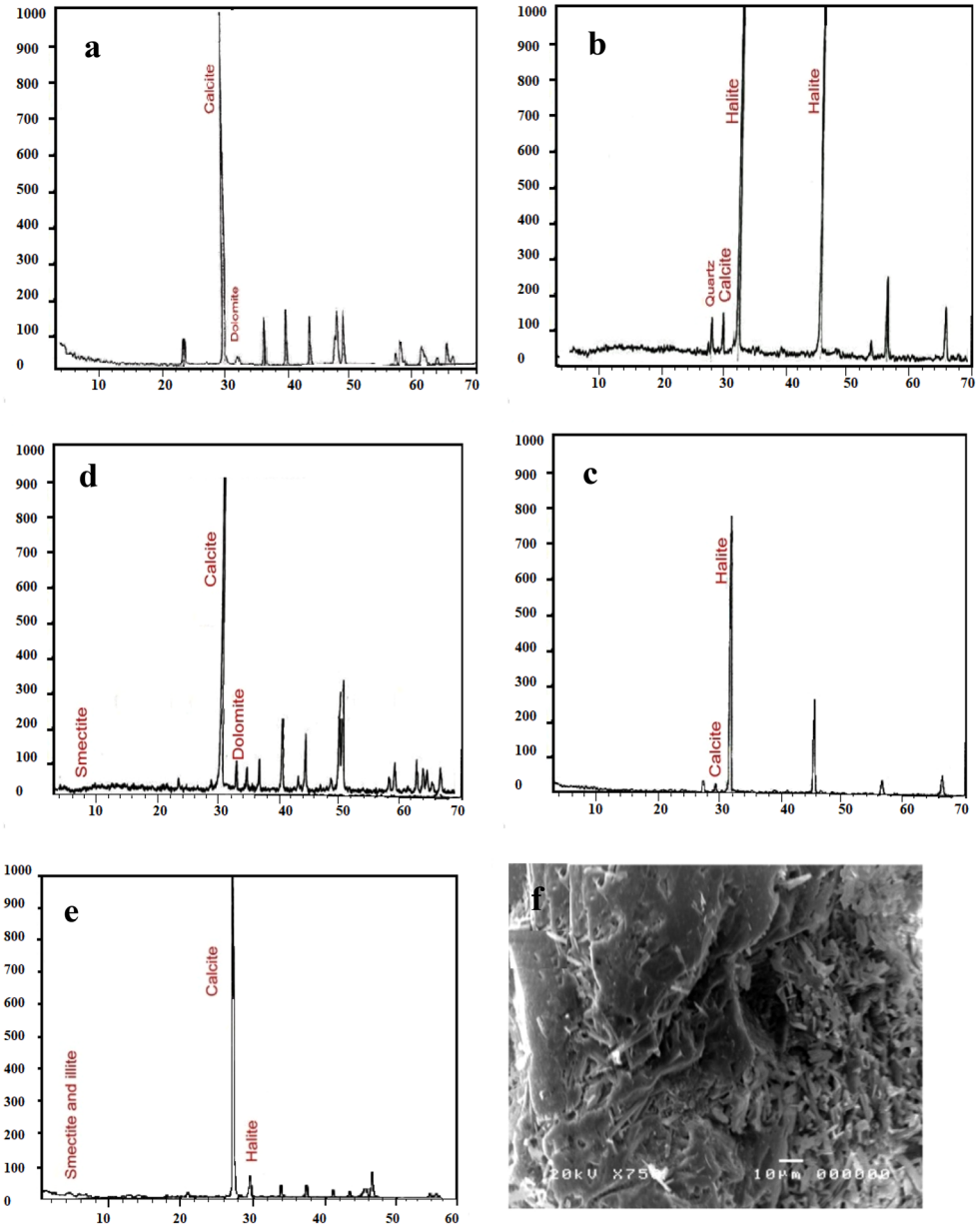

Fig.5 **a**, **b** XRD patterns of limestone and salt samples from the Merit Amun statue, **c**, **d** XRD patterns of limestone and salt samples from the Ramses II statue, and **e**, **f** XRD patterns and SEM photomicrographs (750X) of limestone samples from the colossal seated statue of Ramses II

indicates that there is a tendency for calcite and aragonite to precipitate onto artifact surfaces. This can lead to mineral growth or cementation, which may alter the appearance or structure of the artifacts over time.

The negative saturation indices for dolomite suggest that the groundwater is undersaturated with respect to dolomite. This indicates a higher possibility of dolomite dissolution. This is a concern because the rock artifacts unearthed from the temple are primarily composed of dolomite (Fig. 5a, c). Erosion can lead to the dissolution of limestone, which may cause etching, pitting, or other forms of surface deterioration.

On the other hand, the positive saturation indices of halite indicate that the groundwater has a strong tendency to precipitate these minerals, and this explains the presence of scales and deposits of halite on the

Table 4 Chemical analysis and saturation indices of groundwater in the urban area and the wilderness area around the Open-Air Museum (mg/L)

Sample	1	2	3	4	5
Latitude	26°33′57.83″N	26°33′27.82″N	26°34′3.71″N	26°34′17.63″N	26°33′29.713″N
longitude	31°44′46.16″E	31°44′34.53″E	31°44′37.17″E	31°45′35.26″E	31°43′25.385″E
Class	Urban area	Urban area	Urban area	Wilderness area	Wilderness area
TDS	993	889	959	408	438
HCO_3	384	444	383	251	278
NH_3	14	0.01	0.01	22.5	14.51
Ca	77.15	59.83	72.45	52.29	57.06
K	4	8	6	7	3
Mg	31	17.7	19.07	21	22
Na	188	200	183	42	50
Cl	134.0	113.32	122.52	27.48	34
NO_3	18.23	7.72	125.8	0.21	1.14
So_4	166	119.8	94.61	39	42
PO_4	< 0.2	< 0.2	< 0.2	3.4	0.22
Saturation index (SI)*					
Dolomite	− 8.07	− 9.18	− 8.48	− 10.30	− 9.84
Calcite	1.24	0.96	1.15	0.83	0.90
Aragonite	1.19	0.92	1.11	0.80	0.87
Gypsum	− 0.61	− 0.68	− 0.55	− 0.90	− 0.84
Anhydrite	− 0.76	− 0.85	− 0.71	− 1.11	− 1.04
Halite	4.06	4.75	4.29	5.76	5.47

* A positive value indicates supersaturation, meaning the mineral is more likely to precipitate, while a negative value indicates undersaturation, meaning the mineral is more likely to dissolve

surfaces of the artifacts unearthed from the temple (Fig. 5b, d, e, f). The high pressure generated by the crystallization of halite within the pores of archaeological building materials can cause the minerals to expand during crystallization, leading to dissociation and cracking of the materials.

Protecting the Ramses II temple from urban expansion

To protect the temple from urban expansion, it is necessary to conduct geophysical studies to discover the remaining parts and expedite excavations to preserve whatever is left of the temple before it deteriorates completely. This requires the removal of all buildings surrounding the unearthed part of the temple, which is currently challenging due to the high economic cost. The authors have presented a proposal to protect the temple until the excavation begins. This proposal is based on two steps: The first step is to create an initial visualization of the dimensions of this temple beneath the urban area, and the second step is to establish a protection zone around the temple.

A. Preliminary visualization of the temple's dimensions

Based on the locations of the discovered parts of the temple and the designs of the temples during the reign of Ramses II, a preliminary visualization of the temple's dimensions was made using GIS techniques and a high-resolution satellite imagery.

The discovered parts of the Akhmim temple includes the foundation walls of a Ramesside gate, a colossal statue of Ramses II's daughter Merit-Amun, a statue of Ramses II, and the remains of a colossal statue of Ramses II seated on the throne, which were discovered in 1991 (Fig. 6a). Furthermore, a geophysical survey conducted by [51] in 2009 revealed the existence of another colossal statue seated to the right of this statue. Figure 6b shows the locations of the discovered parts of the Akhmim temple using a WorldView-3 satellite image.

Ramses II constructed numerous temples, but only three of them, namely Abydos temple, Abu Simbel temple, and Ramesseum temple, retained their construction plan. Abu Simbel temple has a unique design as it is a rock-cut temple. Abydos temple and Ramesseum temple showcase the temple design prevalent during the reign of Ramses II. Therefore, it is probable that the temple of Ramses II in Akhmim had a similar design.

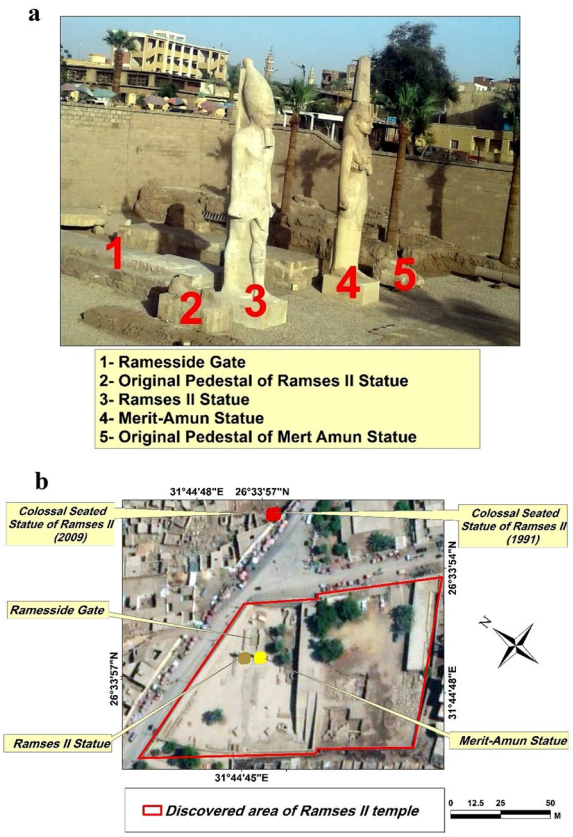

Fig.6 **a** The discovered parts of Ramses II temple (field trip in March 2021), **b** Locations of the discovered parts of the temple by WorldView-3 satellite image

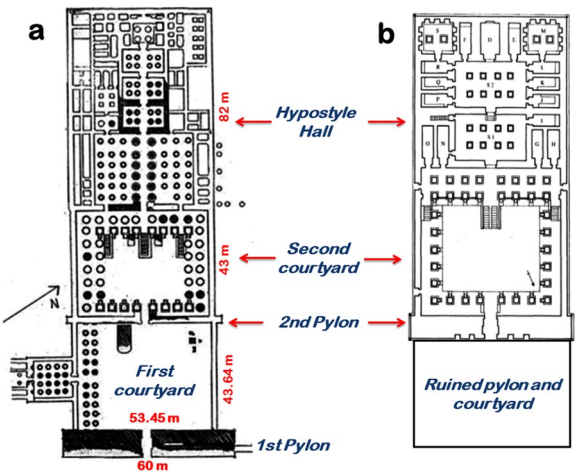

Fig.7 **a** Plan of the Ramesseum temple temple [72], and **b** Plan of the temple of Ramses II at Abydos [75]

The Ramesseum temple, situated in Upper Egypt on the west bank of the River Nile, opposite to the modern city of Luxor, served as a model for subsequent temples, notably the temple of Ramses III at Medinet Habu [72]. According to [73] and [72], the main features of the Ramesseum temple include two massive pylons each leading to a courtyard, the first courtyard ending with a colossal statue of Ramses II, the second courtyard having porticos on all four sides, and the hypostyle hall containing 48 columns arranged in six rows (Fig. 7A). The Abydos temple is situated in Sohag Governorate, Upper Egypt. According to [74], the main features of this temple include a ruined pylon and courtyard at the front, a second courtyard decorated with colossal statues of Ramses II, as seen at the Ramesseum, and a portico (Fig. 7B).

Based on the locations of the discovered parts of the temple and the design of temples during the reign of Ramses II, a preliminary visualization of the dimensions of the Akhmim temple can be made at the following points (Fig. 8):

- The Akhmim temple consists of two pylons, with the Ramesside gate serving as the gateway to the first pylon.
- In front of the first pylon, the Merit-Amun statue and Ramses II statue stand.
- The seated colossal statues of Ramses II, which were discovered in 1991 and indicated by geophysical studies in 2009, were in front of the second pylon.
- Based on the distance between the first pylon and the second pylon (about 63 m) and by analogy with the design of the Ramesseum temple, it can be concluded that the first pylon of Akhmim temple is about 80 m long and the first and second courtyard measure about 73 m wide, and 63 m long. Furthermore, the hypostyle hall and other parts of the temple extend more than 100 m behind the second courtyard.

B. Establishing protection zone around the temple

To ensure the preservation of the temple, it is necessary to establish a protection zone around it, maintaining a distance of 100 m in all directions (Fig. 9). Within this designated protection area, stringent security measures should be implemented to deter unauthorized excavation. Additionally, sewage networks should be installed to prevent water seepage. Prior to any future development within the protection zone, thorough archaeological exploration must be conducted, enabling the documentation of any archaeological findings.

Conclusions

In this study, we examined the urban sprawl of Akhmim city and its impact on the buried temple of Ramses II. The analysis of satellite images clearly illustrates the significant expansion of urban areas around the temple

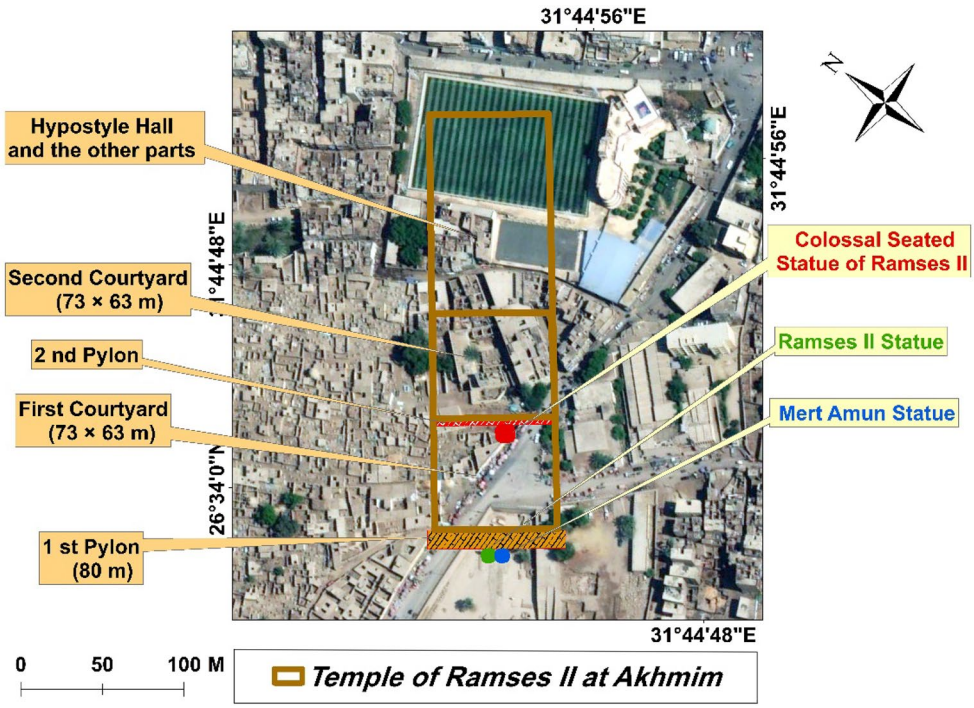

Fig.8 Reconstruction of Ramses II temple in Akhmim city by WorldView-3 satellite image

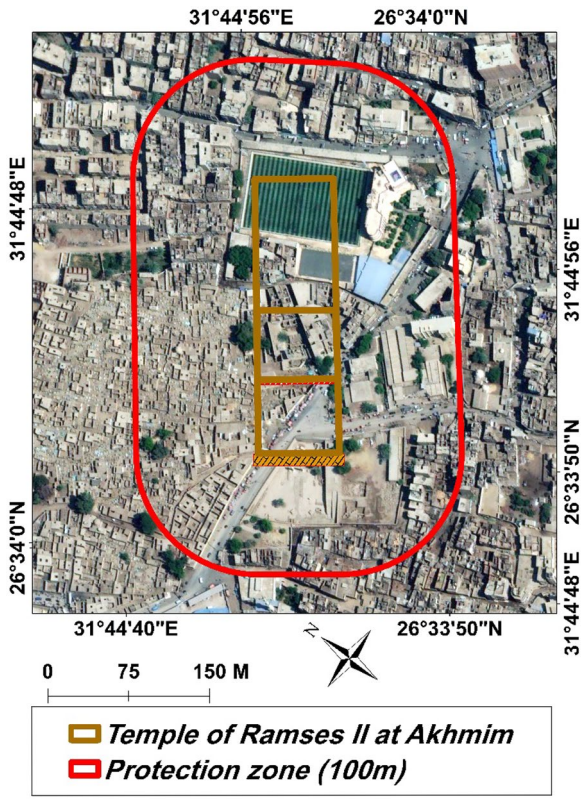

Fig.9 Proposed protection zone around the temple by WorldView-3 satellite image

site over time, particularly after the construction of the Aswan High Dam in 1970. This urban expansion, driven by factors such as population growth and economic opportunities, poses significant challenges to the preservation and management of the temple.

The analysis of archaeological building materials revealed that they are primarily composed of limestone. Sodium chloride (halite) was found, likely originating from burial soil, groundwater, and sewage seepage from nearby homes. The groundwater contains high levels of dissolved solids, chloride ions, and nitrates, which can cause discoloration, warping, and structural damage to archaeological building materials.

Saturation indices for minerals in groundwater indicate a high tendency for dolomite dissolution, which is a concern since the rock artifacts unearthed from the temple are composed of dolomite. On the other hand, there is a high tendency for halite precipitation, explaining the presence of scales and deposits on the surfaces of the artifacts. This process can even lead to disintegration and cracking of materials due to the high pressure resulting from the crystallization of saturated minerals within the pores.

A preliminary visualization of the temple's dimensions beneath the urban area has been presented, based on the discovered parts and the designs of temples during Ramses II's reign. This visualization offers valuable insights into the layout and potential dimensions of

the temple, providing assistance in future excavation and preservation endeavors. We recommend the establishment of a protection zone surrounding the temple where this zone would act as a buffer to protect the temple from encroaching urban development. Implementing stringent security measures to prevent unauthorized excavation and installing sewage networks to mitigate water seepage are crucial steps to be taken within this zone.

This research provides valuable insights into the challenges faced by cultural heritage sites due to urban sprawl and offers practical solutions for their protection and conservation. By prioritizing proactive measures, such as the visualization of temple dimensions and the establishment of protection zones, the preservation of the buried temple of Ramses II in Akhmim city can be assured for future generations. It is crucial that stakeholders and authorities collaborate to implement these measures and safeguard the cultural heritage that enriches our understanding of the past.

Author contributions

MH: conceptualization, methodology, software, writing—original draft preparation, writing and editing. AA: building materials analysis, validation. AAM: reviewing and editing. SFE: reviewing and editing.

Funding

Open access funding provided by The Science, Technology & Innovation Funding Authority (STDF) in cooperation with The Egyptian Knowledge Bank (EKB).

Availability of data and materials

Data sharing is not applicable to this article, as no datasets were generated or analyzed during the current study.

Declarations

Ethics approval consent to participate

Not applicable.

Competing interests

The authors declare that they have no competing interests.

Received: 7 May 2023 Accepted: 22 July 2023
Published online: 16 August 2023

References

1. Frey BS, Steiner L. World Heritage List: does it make sense? Int J Cult Polic. 2011;17(5):555–73.
2. UNESCO. Cultural heritage: 7 successes of UNESCO's preservation work. How to protect cultural heritage? From safeguarding World Heritage sites to recognizing intangible heritage and supporting the creative economy. 2022. UNESCO: https://www.unesco.org/en/cultural-heritage-7-successes-unescos-preservation-work. Accessed 7 mar 2022.
3. Bleibleh S, Awad J. Preserving cultural heritage: shifting paradigms in the face of war, occupation, and identity. J Cult Herit. 2020;44:196–203.
4. Sesana E, Gagnon AS, Ciantelli C, Cassar J, Hughes JJ. Climate change impacts on cultural heritage: a literature review. Wiley Interdiscip Rev: Clim Chang. 2021;12(4):e710.
5. Rosselló J, Becken S, Santana-Gallego M. The effects of natural disasters on international tourism: a global analysis. Tour Manag. 2020;79:104080.
6. Spezzano P. Mapping the susceptibility of UNESCO world cultural heritage sites in Europe to ambient (outdoor) air pollution. Sci Total Environ. 2021;754:142345.
7. Narducci J, Quintas-Soriano C, Castro A, Som-Castellano R, Brandt JS. Implications of urban growth and farmland loss for ecosystem services in the western United States. Land Use Policy. 2019;86:1–11.
8. Meskell L. Sites of violence: terrorism, tourism, and heritage in the archaeological present. In: Meskell L, Pels P, editors. Embedding ethics. Abingdon: Routledge; 2020.
9. Elgendy K, Abaza N. Urbanization in the MENA region: a BENEFIT or a curse. Friedrich Ebert Stiftung, Bonn, Germany; 2020.
10. Revi A, Anguelovski I, Leal Filho W, Olazabal M, Chu E, Cooper JT, Nelson DR. Transformative adaptation in cities. One Earth. 2020;3(4):384–7.
11. Kuddus MA, Tynan E, McBryde E. Urbanization: a problem for the rich and the poor? Pub Health Rev. 2020;2020(41):1–4.
12. Al-Houdalieh S, Sauders R. Building destruction: the consequences of rising urbanization on cultural heritage in the Ramallah Province. Int J Cult Property. 2009;16:1–23.
13. Xie Y, Yang R, Liang Y, Li W, Chen F. The spatial relationship and evolution of world cultural heritage sites and neighbouring towns. Remote Sens. 2022;14(19):4724.
14. UNESCO. List of factors affecting the properties. UNESCO. 2008: https://whc.unesco.org/en/factors/. Accessed 5 Jan 2022
15. Masoumi H, Hosseini M, Gouda A. Drivers of urban sprawl in two large middle-eastern countries: literature on Iran and Egypt. Human Geographies. 2018;12(1):55–80.
16. Ray N, Nikolaus J. Changing Urban environments and the impact on coastal cultural heritage at Marsa Matruh, Egypt. J Maritime Archaeol. 2022;17(3):445–64.
17. Osman T, Shaw D, Kenawy E. An integrated land use change model to simulate and predict the future of greater Cairo metropolitan region. J Land Use Sci. 2018;13(6):565–84.
18. Abouelmagd D, Elrawy S. Cultural heritage and sustainable urban development: the case of Port Said City in Egypt. Cogent Socl Sci. 2022;8(1):2088460.
19. Chyla J. How can remote sensing help in detecting the threats to archaeological sites in Upper Egypt? Geosciences. 2017;7:97.
20. Amato F, Martellozzo F, Nolè G, Murgante B. Preserving cultural heritage by supporting landscape planning with quantitative predictions of soil consumption. J Cult Herit. 2017;23:44–54.
21. Sass O, Viles H. Heritage hydrology: a conceptual framework for understanding water fluxes and storage in built and rock-hewn heritage. Herit Sci. 2022;10(1):1–18.
22. Ahmed AA, Fogg GE. The impact of groundwater and agricultural expansion on the archaeological sites at Luxor, Egypt. J Afr Earth Sci. 2014;95:93–104.
23. Megahed H. Hydrological and archaeological studies to detect the deterioration of Edfu temple in Upper Egypt due to environmental changes during the last five decades. SN Appl Sci. 2020;2:1952.
24. Hemeda S. Finite element assessment FEA of polymer anti-seismic piling techniques for protection of the underground culture heritage. Herit Sci. 2022;10(1):35.
25. UNESCO. Culture urban future: global report on culture for sustainable urban development. Massgraficc & Dhita: 2016.
26. Cardell C, Benavente D, Rodriguez-Gordillo J. Weathering limestone building material by mixed sulfate solutions. charaterization of stone microstructure, reaction products and decay forms. Mater Charact. 2008;59:1371–85.
27. Moustafa SS, Mohamed GEA, Elhadidy MS, Abdalzaher MS. Machine learning regression implementation for high-frequency seismic wave attenuation estimation in the Aswan reservoir area. Egypt Environ Earth Sci. 2023;82(12):307.
28. Abdalzaher MS, Moustafa SS, Hafiez HA, Ahmed WF. An optimized learning model augment analyst decisions for seismic source discrimination. IEEE Trans Geosci Remote Sens. 2022;60:1–12.
29. Abdalzaher MS, Moustafa SS, Abd-Elnaby M, Elwekeil M. Comparative performance assessments of machine-learning methods for artificial seismic sources discrimination. IEEE Access. 2021;9:65524–35.

30. Basheer S, Wang X, Farooque AA, Nawaz RA, Liu K, Adekanmbi T, Liu S. Comparison of land use land cover classifiers using different satellite imagery and machine learning techniques. Remote Sens. 2022;14(19):4978.
31. Nolè G, Murgante B, Calamita G, Lanorte A, Lasaponara R. Evaluation of urban sprawl from space using open-source technologies. Ecol Inform. 2015;26:151–61.
32. Rowlands A, Sarris A. Detection of exposed and subsurface archaeological remains using multi-sensor remote sensing. J Archaeol Sci. 2007;34:795–803.
33. El-Asmar HM, El-Eraky TH, Taha M. El-Gendi Fortress: a new military and religious geo-archaeological site, Sinai, Egypt: geomorphological and hydrogeological remarks. Herit Sci. 2023;11(1):3.
34. Hadjimitsis D, Agapiou A, Alexakis D, Sarris A. Exploring natural and anthropogenic risk for cultural heritage in Cyprus using remote sensing and GIS. Int J Digit Earth. 2013;6(2):115–42.
35. Hemeda S. Geo-environmental monitoring and 3D finite elements stability analysis for site investigation of underground monuments Horemheb tomb (KV57), Luxor Egypt. Herit Sci. 2021;9(1):17.
36. Shams eldein A, Elfadaly A, Wafa O, Abouarab M, Attia W, Hagage M, et al. Geo-environmental risk assessment around Qayitbay castle, Rosetta, Egypt, using remote sensing and GIS techniques. مجلة العمارة و الفنون و العلوم الإنسانية, 2018;3(11): 1–17.
37. Parcak S, Mumford G, Childs C. Using open access satellite data alongside ground based remote sensing: an assessment, with case studies from Egypt's delta. Geosciences. 2017;7:94.
38. Nsanziyera A, Rhinane H, Oujaa A, Mubea K. GIS and remote-sensing application in archaeological site mapping in the Awsard Area (Morocco). Geosciences. 2018;8:207.
39. Oonk S, Slomp CP, Huisman DJ. Geochemistry as an aid in archaeological prospection and site interpretation: current issues and research directions. Archaeol Prospect. 2009;16(1):35–51.
40. Hermann A, Forkel R, McAlister A, Cruickshank A, Golitko M, Kneebone B, Mark McCoy M, Reepmeyer C, Sheppard P, Sinton J, Weisler M. Pofatu, a curated and open-access database for geochemical sourcing of archaeological materials. Sci Data. 2020;7(1):141.
41. Ahmed H, Mahgoub G, Mohamed S, Elnaggar A. Archaeometallurgical characterization and condition assessment of Ancient Roman coins from Egypt. Shedet. 2021;8(8):149–67.
42. Ponce-Antón G, Arizzi A, Zuluaga MC, Cultrone G, Ortega LA, Agirre MJ. Mineralogical, textural and physical characterisation to determine deterioration susceptibility of Irulegi Castle lime mortars (Navarre, Spain). Materials. 2019;12(4):584.
43. Yan R, Zhu J, Xi F, Chen A. Development and application of a hydrogeochemical model for the groundwater treatment process in waterworks. Water. 2022;14(13):2103.
44. Kuhlmann K. Materialien zur ärchaeologie und geschichte des raumes von Achmim. SDAIK. 1983;11:61–78.
45. Hafez M. Akhmim, "Panopolis" in the Graeco-Roman period: a historical, archaeological study and local touristic development. J Fac Tour Hotel-Univ Sadat City. 2020;4(2):94–110.
46. Elias J. The Encyclopedia of Ancient History. Oxford; 2013.
47. Jackson BC. Akhenaten and His Aten Cult in Abydos and Akhmim. In: Bonnet C, Galoppin T, Guillon E, Luaces M, Lätzer-Lasar A, Lebreton S, Porzia F, Rüpke J, Rubens Urciuoli E, editors. Naming and mapping the Gods in the ancient mediterranean. Berlin: De Gruyter; 2022.
48. Rawlinson G. The History of Herodotus. London; 1949.
49. Abdel Nasser G, Baumann S, Leitz C. A newly discovered edifice of Atum in Akhmim part of the necropolis of the primeval gods? ENIM. 2015;8:187–221.
50. Britannica, The Editors of Encyclopaedia. "Akhmīm". Encyclopedia Britannica. 2017. https://www.britannica.com/place/Akhmim. Accessed 6 Apr 2023.
51. Hafez M, Atya M, Hassan A, Sato M, Wonik T, El-Kenawy A. Shallow geophysical investigations at the Akhmim archaeological site, Suhag Egypt. Appl Geophys. 2008;5(2):136–43.
52. Brereton RG, Lloyd GR. Support vector machines for classification and regression. Analyst. 2010;135(2):230–67.
53. Kebede TA, Hailu BT, Suryabhagavan KV. Evaluation of spectral built-up indices for impervious surface extraction using sentinel-2A MSI imageries: a case of addis Ababa City. Ethiop Environ Chall. 2022;8:112.
54. Rumora L, Miler M, Medak D. Impact of various atmospheric corrections on sentinel-2 land cover classification accuracy using machine learning classifiers. ISPRS Int J Geo-Inf. 2020;9:277.
55. Richards JA. Remote sensing digital image analysis: an introduction. Berlin/Heidelberg: Springer; 2013.
56. Talukdar S, Singha P, Mahato S, Shahfahad Pal S, Liou Y, et al. Land-use land-cover classification by machine learning classifiers for satelliteobservations—a review. Remote Sens. 2020;12:1135.
57. Petropoulos GP, Kalaitzidis C, Prasad VK. Support vector machines and object-based classification for obtaining land-use/cover cartography from hyperion hyperspectral imagery. Comput Geosci. 2012;41:99–107.
58. Maxwell AE, Warner TA, Fang F. Implementation of machine-learning classification in remote sensing: an applied review. Int J Remote Sens. 2018;39:2784–817.
59. Kavzoglu T, Colkesen I. A kernel functions analysis for support vector machines for land cover classification. Int J Appl Earth Obs Geoinf. 2009;11:352–9.
60. Mann D, Joshi PK. Evaluation of image classification algorithms on hyperion and ASTER data for land cover classification. Proc Natl Acad Sci India Sect A Phys Sci. 2017;87(4):855–65.
61. Appelo CAJ, Postma D. Geochemistry, groundwater and pollution. Boca Raton: CRC Press; 2004.
62. Zajac M, Skocek J, Lothenbach B, Mohsen BH. Late hydration kinetics: Indications from thermodynamic analysis of pore solution data. Cem Concr Res. 2020;129:105975.
63. Tyagi S, Sarma K. Qualitative assessment, geochemical characterization and corrosion-scaling potential of groundwater resources in Ghaziabad district of Uttar Pradesh, India. Groundw Sustain Dev. 2020;10:100370.
64. Hajirezaie S, Wu X, Soltanian MR, Sakha S. Numerical simulation of mineral precipitation in hydrocarbon reservoirs and wellbores. Fuel. 2019;238:462–72.
65. Amrani S, Hinaje S, El Fartati M, Gharmane Y, Yaagoub D. Assessment of groundwater quality for drinking and irrigation in the Timahdite-Almis Guigou area (Middle Atlas, Morocco). Appl Water Sci. 2022;12(4):82.
66. Madani A, Hagage M, Elbeih SF. Random forest and logistic regression algorithms for prediction of groundwater contamination using ammonia concentration. Arab J Geosci. 2022;15(20):1619.
67. Elbeih SF, Madani AA, Hagage M. Groundwater deterioration in Akhmim district, Upper Egypt: a remote sensing and GIS investigation approach. Egypt J Remote Sens Space Sci. 2021;24:919–32.
68. Hagage M, Madani AA, Elbeih SF. Quaternary groundwater aquifer suitability for drinking in Akhmim, Upper Egypt: an assessment using water quality index and GIS. Arab J Geosci. 2022;15:196.
69. Fahmy A, Molina-Piernas E, Martínez-López J, Domínguez-Bella S. Salt weathering impact on nero/Ramses II temple at El-Ashmonein archaeological site (Hermopolis Magna). Egypt Herit Sci. 2022;10(1):125.
70. Li P, Du M. Effect of chloride ion content on pitting corrosion of dispersion-strengthened-high-strength steel. Corros Commun. 2022;7:23–34.
71. Warscheid T, Braams J. Biodeterioration of stone: a review. Int Biodeterior Biodegrad. 2000;46(4):343–68.
72. Lecuyot G. The Ramesseum (Egypt), recent archaeological research. Paris: CNRS; 2012.
73. Leblanc C. Research, development and management of heritage on the left bank of the Nile: Ramesseum and its environs. Museum Int. 2005;57(1):79–86.
74. Abdelrahiem M. The festival court of the temple of Ramesses II at abydos (Part I). Stud zur Altägyptischen Kultur. 2010;39:1–17.
75. Breitenstein R. Ein tempel für millionen von jahren: Ein ikonographischer rundgang durch den temple Ramses' II, in Abydos (A Temple for Millions of Years: An Iconographic Tour of the Temple of Ramses' II, in Abydos). Antike Welt. 1999;30(6):555–63.

Publisher's Note